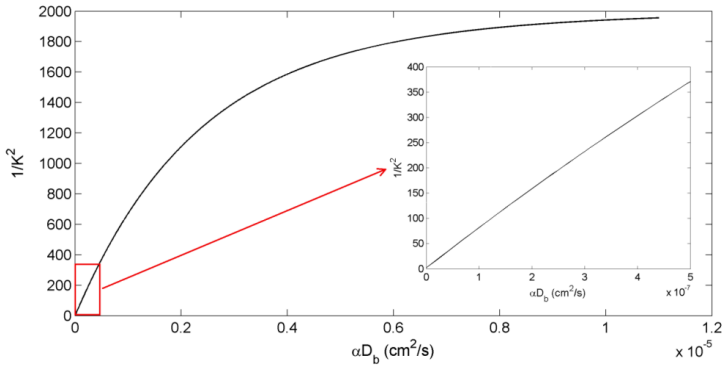

Fig. 1. Theoretical calculation of $1/K^2$ as a function of αD_b over a broad range. Red box region, which is magnified in the inlet, refers to the region where αD_b is in the physiological range. A good linearity is observed between $1/K^2$ and αD_b within the physiologically relevant region. In this simulation, $\mu_s' = 8$ cm^{-1}, $\mu_a = 0.03$ cm^{-1}, $\beta = 0.5$, and the exposure time of 0.2 ms was used.

We used the similar optical properties as human tissue, where $\mu_s' = 8$ cm^{-1} and $\mu_a = 0.03$ cm^{-1}. From the simulation result, $1/K^2$ is shown to be an increasing function of αD_b, with a gradually decreasing slope. However, in the lower range of αD_b, the relation is close to linearity. Fortuitously, the reported physiologically relevant maximum values of *in vivo* αD_b are located in the approximate linear range (~1×10^{-6} cm^2/s) [4, 7, 8, 10, 29]. This is the theoretical basis for DSCA that $1/K^2$ can be used as a substitute for the conventional BFI in DCS.

We have shown the spatial speckle contrast K_s can be used for rBF measurement in our previous work [1]. Since there is no fundamental difference between K_s and K_t, we build our fiber based multi-channel *t*DSCA device on the same theoretical basis.

3. Instrument and method

In our 3-channel *t*DSCA setup, the light source is a continuous-wave laser with a long coherence length (>10 meter) operating at 785 nm (DL785-100-S, ~100mW, CrystaLaser, Reno, Nevada, USA). A high quality VGA camera (Stingray F033, Allied Vision Technology) is used as detector. As shown in Fig. 2(a), the laser source is divided equally into four multi-mode fibers with three cascading 50:50 fiber splitters, where three of them are used as source fibers in the probes, and the other one is used for source power monitoring. Three single mode fibers are used as detector fibers in the probes, with the other ends touching onto the CCD chip directly. The CCD camera is controlled by a laptop, with LabVIEW program (National Instrument).

We set the frame rate at 60 fps, and calculate $1/K_t^2$ every 1 second with 60 data points. Thus the update rate for *t*DSCA system is 1 Hz. The moving average of $1/K_t^2$ with a window size of 4 is applied for further data smoothing.

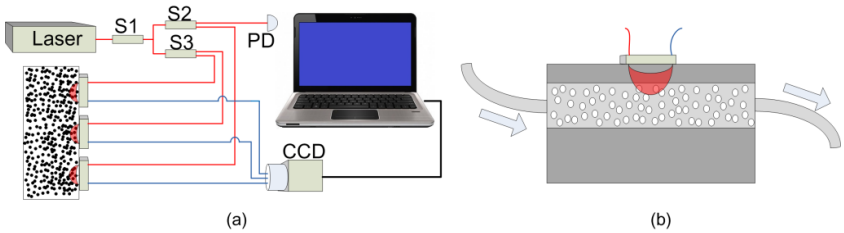

Fig. 2. Schematic of (a) *t*DSCA setup and (b) the phantom experiment. S1, S2 and S3 are 50:50 fiber splitters, PD is photon detector for power monitoring. Small glass beads are filled inside the hollow tube which is embedded in the solid phantom to provide randomized interstitial space for the flow.

#191766 - $15.00 USD Received 12 Jun 2013; revised 10 Aug 2013; accepted 6 Sep 2013; published 20 Sep 2013

To test the 3-channel *t*DSCA device, we performed a flow-controlled phantom experiment. The optical properties of the solid phantom were $\mu_s' = 8$ cm^{-1} and $\mu_a = 0.03$ cm^{-1}, as described in our previous work [6]. As shown in Fig. 2(b), a hollow tube was embedded inside the solid body, and was tightly filled up with small glass beads to provide randomized interstitial space for the flow. To mimic the blood, we diluted Lipofundin N 20% (B.Braun Melsungen AG, Germany) into concentration of 0.6%. A peristaltic pump was used to control the flow rate inside the tube.

Before the *t*DSCA test, we performed DCS measurement on the upper surface of the phantom by our software correlator-based DCS system [6], with a source-detector separation of 3 cm. The flow rate was controlled from 0 to 0.35 ml/s, in steps of 0.05 ml/s.

Then we located each *t*DSCA probe in the same position as that of DCS probe, and tested them one by one with the same flow-control protocol. These three tests can be regarded as independent. The exposure time was 0.2 ms. The results will be shown in the next section.

4. Result

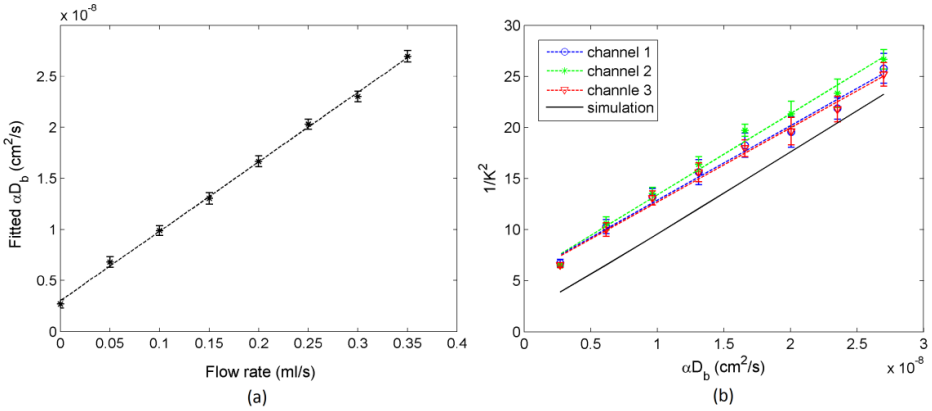

Fig. 3. (a) Relationship between αD_b and flow rate measured by DCS on the flow phantom. (b) Dependence of $1/K^2$ on BFI, measured on three different *t*DSCA channels. Note the x-axis is αD_b not flow rate, as we converted flow rate into αD_b using the linear relationship shown in Fig. 3(a). The simulation result from Eqs. (2)-(3) is also plotted in (b) for comparison.

Figure 3(a) shows the result from DCS measurement on flow phantom. Under Brownian motion assumption, the fitted αD_b is very linear to the flow rate with a small offset. This offset value observed for zero flow is attributable to both innate Brownian motion of the particles inside the phantom and the inherent source fluctuation. We also observed very similar result in our previous work [6] with the same flow phantom, where we also confirmed the Brownian motion model gives better fitting than the random flow model. Therefore, the Fig. 3(a) can be regarded as a calibration curve between the flow rate and D_b in our particular flow phantom, and it enables us to make comparison between the simulation result and the experimental *t*DSCA result. In Fig. 3(b), experimental results on three different channels are shown in different colors, and they almost overlap with each other showing very good consistency. Simulation result using Eqs. (2)-(3) is also shown for comparison, and both experimental and simulation results are in the same order of magnitudes and have similar slopes.

After the validation study using flow phantom, we performed *in vivo* experiment on human forearm and palm using cuff occlusion protocol, with exposure time of 0.2 ms. Two probes were placed on the surface of the inside of forearm, and one more probe was placed on the surface of the hypothenar area, with the same source-detector separation of 1.5 cm. During the experiment, we measured the baseline for 100 s. Then a cuff occlusion was applied on upper arm with a pressure of 200 mmHg for about 75 s, which would lead to a

#191766 - $15.00 USD Received 12 Jun 2013; revised 10 Aug 2013; accepted 6 Sep 2013; published 20 Sep 2013

dramatic decrease of blood flow in the forearm and palm. Finally the pressure was released, and the recovery period was also recorded.

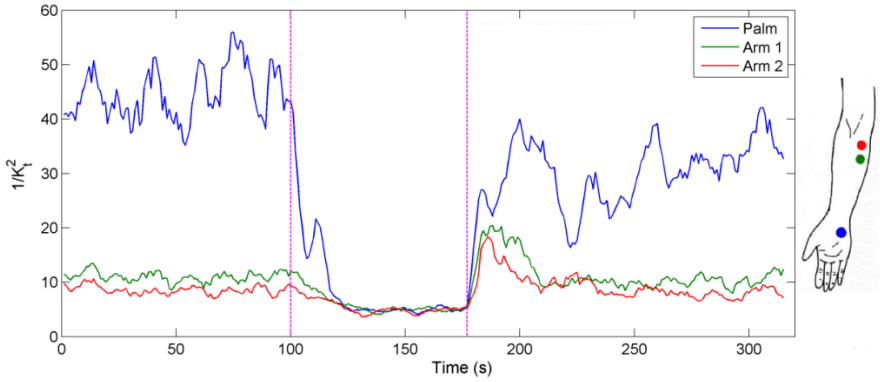

Fig. 4. Results from 3-channel tDSCA system during *in vivo* experiment with arm-cuff protocol. The positions of the three probes are indicated by corresponding colors on the arm.

The responses from three channels are plotted in Fig. 4. The two channels on forearm show very similar response, while the other channel on palm shows much higher blood flow reading during baseline. The palm channel also shows quite different reactive hyperemia pattern than the other two after the release of the cuff. However, the results from all channels are very similar in amplitude during cuff occlusion period, during which the microcirculation becomes minimal.

The higher baseline BFI in palm can be explained by the presence of many well-perfused small muscles in palm, which makes the palm look red. During arterial cuff occlusion, however, the blood flow underneath the skin is very low in the whole upper limb equally, because the blood supply is blocked. Thus there is little difference of BFI among all channels during cuff occlusion.

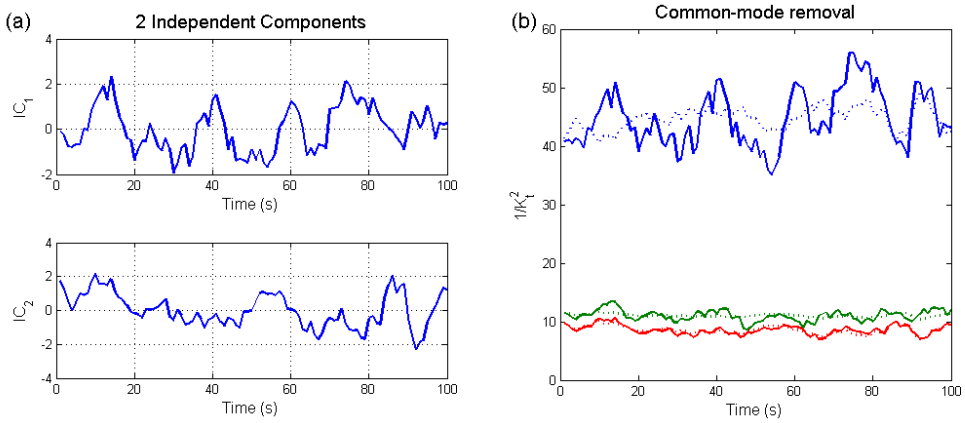

Fig. 5. Example of independent component analysis (ICA) performed on the first 100s *t*DSCA data shown in Fig. 4. (a) Two independent components resulting from iterative ICA algorithm, displayed after centering and normalizing. (b) Original 3-channel data (in solid line) overlaid with common-mode removed data (in dotted line) See text for details.

Further analysis can be done on the simultaneous 3-channel data described above. As the three time series data are acquired concurrently, it can be assumed that they are in fact linear combinations of more fundamental modes. We indeed observe similar behaviors among the three channels in the baseline measurement, and performed independent component analysis (ICA) on the first 100s data shown in Fig. 4 assuming there are only two independent components (ICs). ICA is a well-known iterative method to find out a set of source time

#191766 - $15.00 USD Received 12 Jun 2013; revised 10 Aug 2013; accepted 6 Sep 2013; published 20 Sep 2013

series that are most independent of each other, typically used to solve blind source separation problems in audio signals or EEG signals. The results are shown in Fig. 5, where the two ICs are shown in Fig. 5(a), and the original data with common-mode removed data are shown in Fig. 5(b). The common mode that is removed is IC_1 which shows big oscillations with frequencies below 0.1 Hz, that is believed to be the low-frequency oscillation (LFO) related to the waves in vasodilation. This common-mode removal results in much flatter baseline behavior as shown in Fig. 5(b) as dotted lines, proving that ICA is beneficial when dealing with multi-channel concurrent data, as it enables one to separate out different physiologies.

5. Discussion

Compared with our previous work using *s*DSCA [1], the result from *t*DSCA system corresponds much better with the simulation. This is because the single mode fiber has a very small diameter (~4.5 μm), which is comparable to the speckle size. Thus β is close to 0.5. In the three independent tests, it is difficult to guarantee the three probes are exactly in the same position, which may cause the slight difference in slopes in Fig. 3(b).

In DSCA, we can take reference from LSCI on the optimal exposure time issue. It is suggested that the exposure time T should be around τ_c where $g_1(\tau) = 1/e$, to obtain the best sensitivity to particle dynamics [31]. Thus T should be about 0.1~1 ms in typical DSCA measurement. We used exposure time of 0.2 ms in our *t*DSCA system, and it worked properly.

From our simulation result in Fig. 1, there is one-to-one correspondence between αD_b and $1/K^2$, when optical properties, β and exposure time are given. Thus the simulation result can serve as the calibration curve from $1/K^2$ to the BFI in DCS. Because of the approximate linear relationship in physiologically relevant range of αD_b, it is straight forward to use $1/K^2$ to indicate rBF as a function of time for specific site.

The noise-like fluctuation in the baseline of our *in vivo* result is due to the low frequency oscillation (LFO) in normal blood flow regulation, not the instrument noise. The main frequency components (0.06 Hz in palm and 0.07 Hz in arm) correspond well with *in vivo* LFO frequency band [32, 33]. Moreover, during cuff occlusion, the readings are much smoother without obvious fluctuation. This confirms the stability of the *t*DSCA device and certifies that the fluctuation in the baseline origins from blood flow regulation.

We further attempted to separate out the LFO signal from the fluctuating baseline signal using ICA, and the result is promising as shown in Fig. 5. Although one of the positions (palm) is quite far from the other two (arm 1 and arm 2), we were able to see common behaviors among different channels as same brachial artery is responsible for perfusing whole lower arm. We anticipate that a systematic study with more number of channels that cover broader area on human body will result in interesting physiological assessment which is impossible using a single channel perfusion monitoring.

6. Conclusion

In conclusion, *t*DSCA is reported for the first time for deep tissue blood flow measurement, and a cost effective multi-channel *t*DSCA flowmetry device based on single CCD camera is demonstrated. *t*DSCA is clearly a more practical choice for bedside blood flow monitoring on multiple sites than *s*DSCA is. Taking the advantages of simple instrumentation, easy analysis and low cost into account, *t*DSCA can be regarded as a good alternative for DCS.

In the future, high sensitivity and high frame rate CCD can greatly increase the time resolution of *t*DSCA, which will enable observation of fast responses on multiple positions at the same time.

Acknowledgment

This study was partly funded by the Ministry of Education in Singapore, Academic Research Fund Tier 1 grant (RG37/07). The authors wish to thank Dr. Hojin for the inspirational discussion we had.

#191766 - $15.00 USD Received 12 Jun 2013; revised 10 Aug 2013; accepted 6 Sep 2013; published 20 Sep 2013